Fibers and Polymers (2024) 25:1623–1634
https://doi.org/10.1007/s12221-024-00526-3

Online ISSN 1875-0052
Print ISSN 1229-9197

REGULAR ARTICLE

Superhydrophilic and Oil-Resistant SiO_2/PU Fiber Membrane for Oil-In-Water Emulsion Separation under Gravity

Li Gao[1] · Haihong Gu[1] · Chunxia Wang[1] · Huanling Wu[1] · Chao Ye[1]

Received: 27 September 2023 / Revised: 30 January 2024 / Accepted: 7 March 2024 / Published online: 3 April 2024

Abstract

A polyurethane membrane with interlayer channels was developed through electrospinning to separate oily sewage. To enhance its hydrophilicity, hydrophilic silica particles were grafted onto the fiber surface, creating a rough surface. This was done by treating the membrane with oxygen plasma to generate active sites, which were then coupled with 3-aminopropyltriethoxysilane, followed by adding the membrane to a hydrolytic solution of tetraethyl orthosilicate. The resultant membrane had a low water contact angle of 23.3° and excellent underwater oleophobicity, with a high-underwater oil contact angle (varied from 155.9 to 159.7°) and underwater oil sliding angle (ranged from 4.0 to 4.6°) for different types of oils. In addition, the prepared membrane had a good moisture-evaporation rate (4.2 g/h) and water-absorption capacity (273%). It is also oil-resistant and self-cleaning in water, and could efficiently separating oil-in-water emulsion under gravity, with an initial separation flux of 2864 L/m^2/h. During cyclic separation of emulsion, the membrane had the oil-retention rate of more than 99.0%, and the final separation flux of the membrane was maintained at 25 L/m^2/h.

Keywords Polyurethane fiber membrane · Silica graft modification · Superhydrophilic surface · Oil resistance · Oil-in-water emulsion separation

1 Introduction

The treatment of oily wastewater has been a challenging task in recent times [1, 2]. However, the advancement of membrane separation technology has made it possible to effectively and cost-efficiently treat and purify these kinds of wastewater at a large scale [3–5]. This technology is based on the difference in interface between water and oil on the membrane surface. Two-dimensional (2D) laminated membranes fabricated by electrospinning have been proposed for oil–water separation due to their crosslinked fibers and interlayer channels [6, 7]. These fluid channels have great potential for oil–water separation as they can break through the limitation of the membrane pore size [8, 9]. However, the sieving performance can be compromised due to oil contamination during the separation process, resulting in a decrease in the filter membrane's service time due to a drop in separation flux and efficiency [10, 11]. To address this, surface modification methods such as chemical deposition, interface aggregation, surface grafting and layer-by-layer assembly have been used to construct hydrophilic surfaces on the 2D laminar membrane, incorporating a range of biopolymers, ceramic and inorganic nanomaterials [12–14]. In particular, the hydrophilic membrane has been characterized by its low-operating pressure, high filtration flux and good-antifouling performance, which is mainly attributed to the surface structure and chemical composition of the material [15–17].

To improve the antifouling capability of the electrospun membrane, low-temperature plasma technology has been employed to modify various types of materials due to its simple fabrication method and ideal modification of all surfaces without altering their bulk physical properties [18–20]. The surface can be modified by plasma treatment to create active sites, in some cases, even rough surfaces can be formed due to the etching effect of the process [21, 22]. However, the surface modification by the plasma treatment is time-sensitive and the wettability may be lost due to the active groups flipping to the inner side of the molecular chain [23, 24]. The introduction of

✉ Haihong Gu
guhaihong@ycit.edu.cn

✉ Chao Ye
yechao@ycit.edu.cn

[1] College of Textile and Clothing, Yancheng Institute of Technology, Yancheng 224001, China

functional groups through chemical reactions was used to achieve a lasting alteration of the membrane, creating a covalent bond between the grafting chain segment and the membrane surface [25–27]. Moreover, the presence of hydrophilic groups forming hydrogen bonds with water molecules weakened the hydrophobic effect of the pollutants and the membrane surface [28, 29]. Chemical modification and the formation of multi-level structures on the membrane surface resulted in a unique wetting of the membrane, thereby increasing the antifouling property, permeate flux, and separation efficiency [30, 31].

Previously, electrospun polyurethane (PU) membranes were modified to be hydrophobic and used for the separation of oil–water mixtures [32]. However, this preparation process was often time-consuming and required harsh conditions such as high temperature or pressure [33]. In addition, hydrophobic membranes were lipophilic and prone to contamination by oil, thus reducing the service life of the membranes in oil–water separation [34, 35]. Nowadays, a membrane with a porous structure, a rough surface, and a hydrophilic epidermis can be fabricated through plasma treatment, silane coupling, and silica grafting at ambient temperature in combination with ultrasonication. This prepared membrane displays remarkable hydrophilicity, with a low water contact angle (WCA), a high moisture-evaporation rate, and a high water-absorption capacity. In addition, owing to its excellent underwater oleophobicity to various oils, the membrane has a high resistance and low adhesion to oils. Based on the sieving effect of the pore channels and the repulsion of water on the membrane surface to the oil droplets, the resultant membrane can be used to efficiently separate oil-in-water emulsion under gravity.

2 Experiment Section

2.1 Materials

Polyurethane (PU, Elastollan 1190A10) was procured from BASF Polyurethane Co., Ltd. Dimethylformamide (DMF, AR, 99.5%), butyl acetate (BuAc, ACS, ≥99.5%), 3-aminopropyltriethoxysilane (APTES, 98%), tetraethyl orthosilicate (TEOS, 98%), ethanol (AR, 99.7%), sodium dodecyl benzene sulfonate (SDBS, AR, 90%), ammonia solution (AR, 25%), dichloromethane (AR, 99.5%), carbon tetrachloride (98%), bromobenzene (AR, 98%), nitrobenzene (99%), peanut oil, and oil red O were acquired from various suppliers for use in the experiment. Oxygen (O_2, 99.5%) was sourced from Yancheng Guangyuan Gas Co., Ltd. Deionized water was utilized for the preparation of all aqueous solutions.

2.2 Plasma Treatment on PU Fiber Membrane

A PU fiber membrane was electrospun with an average fiber diameter of 878 nm, as previously described [36]. The membrane was then subjected to a low-temperature plasma treatment in a plasma modification processor (HD-1A/B, China). The membrane was placed between two parallel electrodes in a metallic chamber, which was evacuated to a base pressure of 40 Pa and then oxygen (O_2) gas was introduced at a flow rate of 500 sccm. Figure 1a illustrated that

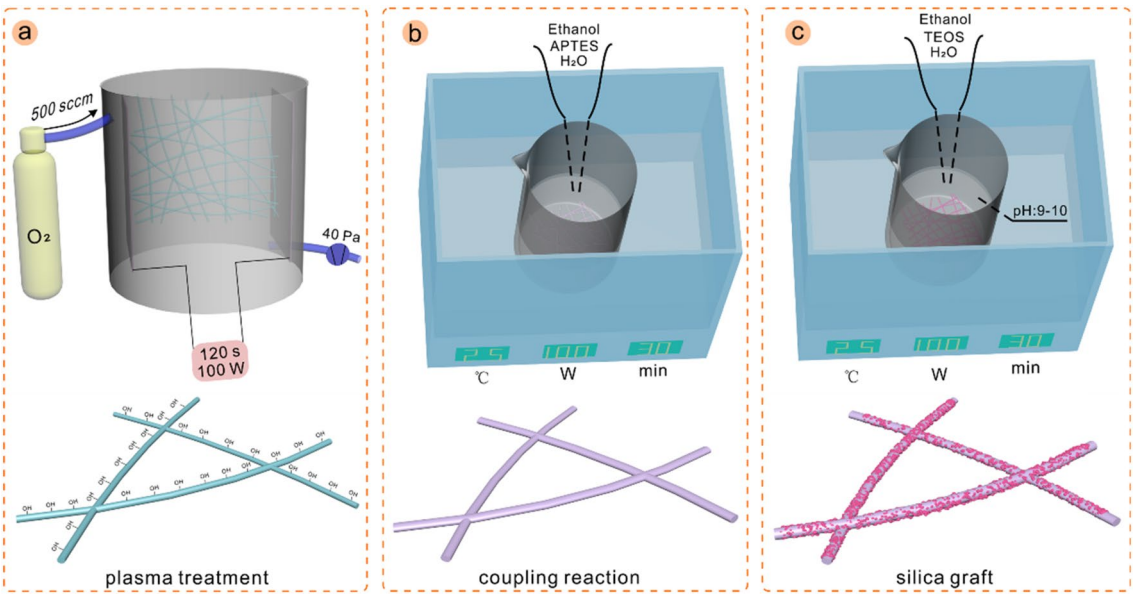

Fig. 1 Schematic illustration of the fabrication process for the superhydrophilic membrane

the membrane was exposed to the plasma treatment for a duration of 120 s while the output power was set to 100 W.

2.3 Hydrophilic Modification

The pre-treated membrane was immersed in a solution of 0.01 M 3-aminopropyltriethoxysilane (APTES) in a mixture of ethanol and water (1:2, v:v) and ultrasonicated for 30 min at an ambient temperature of (25 ± 5) ℃, to promote the coupling of APTES and the membrane (Fig. 1b). Subsequently, the membrane was incorporated into a solution of tetraethyl orthosilicate (TEOS), water, and ethanol in a proportion of 1:2:4, and ultrasonicated for 30 min at an ambient temperature of (25 ± 5) ℃ under a pH of 9–10, to produce a superhydrophilic membrane (Fig. 1c).

2.4 Characterization

The contact angle (CA) was measured using a JCY-4 contact angle meter, while the sliding angle (SA) was determined by a tilting stage method [37]. The rate of moisture evaporation (E_v, g/h) was estimated by the slope of the time–evaporation curve until it reached a plateau [38]. The water-absorption rate (ϕ, %) was implemented according to the GB/T 21655.1–2023 standard test method and calculated using the equation: $\phi = \frac{m_w - m}{m} \times 100$, where ϕ was the water-absorption rate of the membrane, m_w and m were the masses of the absorbed-water membrane and dried membrane, respectively. The morphology and elemental mapping were investigated using a field emission scanning electron microscope (FE-SEM, Nova NanoSEM 450, USA) with an energy dispersive X-ray spectroscopy (EDS). The infrared spectrum of the membrane was obtained using a Fourier transform infrared spectrometer (FTIR, NEXUF-670, USA). The surface element composition was further analyzed by an X-ray photoelectron spectrometer (XPS, EscaLab 250Xi, China). The value of root-mean square roughness (R_q) was determined using an atomic force microscopy (AFM, SPM-9700, Japan). The fiber diameter distribution of membrane and the particle size of silica were counted by Image J software through the SEM image of the membrane. The thickness of the membrane was measured from cross section in the SEM image. The pore size distribution and porosity of the membrane were surveyed using a mercury porosimeter (MIP, Autopore 9600, USA). And the content of silica grafted on the membrane was measured by the equation: $C_s = \frac{m_S - m_A}{m_T + m_S - m_A} \times 100$, where C_s (%) was the content of the silica grafted onto the membrane, m_S (g) was the weight of the membrane grafted with silica, m_A (g) was the weight of the membrane coupled with APTES, and m_T (g) was the weight of silica synthesized by the hydrolysis and condensation of TEOS. The morphology of the emulsion and filtrate was observed by the optical microscope, and the particle size distribution of the emulsified oil was determined using Image J software. In addition, the water flux (J, L/m^2/h) was calculated by measuring the volume of water collected under gravity over a fixed period of time [26]. This was done using the formula: $J = \frac{V}{A \cdot t}$, where V was the volume of water collected by the membrane, A was the effective permeation area (1.767×10^{-4} m^2), and t was the permeation time. The oil-retention rate (R, %) can be calculated by the formula: $R = \left(1 - \frac{C_f}{C_0}\right) \times 100$, where C_f and C_0 are the oil content in the filtrate and the feed emulsions, respectively. And oil content in the separated filtrate was detected by the UV–vis spectrophotometer [39].

3 Results and Discussion

3.1 The Hydrophilicity of the Fiber Membrane

The initial WCA of the electrospun PU membrane was 132.8°, and the water droplet penetrated the membrane under the gravity effect of the water drop and the polar effect of the PU soft segment (Fig. 2a I) [40]. To improve the hydrophilicity of the membrane, low-temperature plasma treatment acted on the surface of the membrane, the water droplet could penetrate the membrane of the initial WCA of 37.2° in 1 s, as shown in Fig. 2a II. Meanwhile, the underwater oil contact angle (UOCA) increased from 20.6 to 150.4° after the plasma treatment of oxygen (O_2) in Fig. 2b I–II. Moreover, the moisture-evaporation rate (E_v) and water-absorption rate (∅) of the plasma-treated membrane increased from 0.12 g/h to 0.27 g/h and from 359 to 519%, respectively (Fig. 2c, d I–II). Compared with the morphology of the electrospun PU fiber surface, the surface of the fiber treated by the plasma did not change evidently, and the surface was also smooth, it meant that the plasma with O_2 at 100 W in 120 s did not etch the fiber surface (Fig. 3a, b) [21]. To achieve the desired and lasting special wettability, APTES as the coupling agent was wrapped on the fiber surface [41], and the fibers were in an adhesive state (Fig. 3c). With the wrapping of APTES, the hydrophilicity of the membrane decreased obviously (the initial WCA of the membrane increased to 118.3°, Fig. 2a III), meanwhile, the membrane lost the underwater superoleophobicity (UOCA dropped to 148.8°, below 150°, Fig. 2b III). Furthermore, the moisture-evaporation rate and water-absorption capacity of the membrane declined obviously (E_v decreased to 0.15 g/h and ∅ declined to 218%, Fig. 2c, d III). And then the hydrophilic silica particles (SiO_2) were synthesized by sol–gel method during the hydrolysis and condensation of TEOS and aggregated on the fiber surface, as shown in Fig. 3d. In addition, it could be found that the average fiber diameter of the SiO_2/PU membrane increased

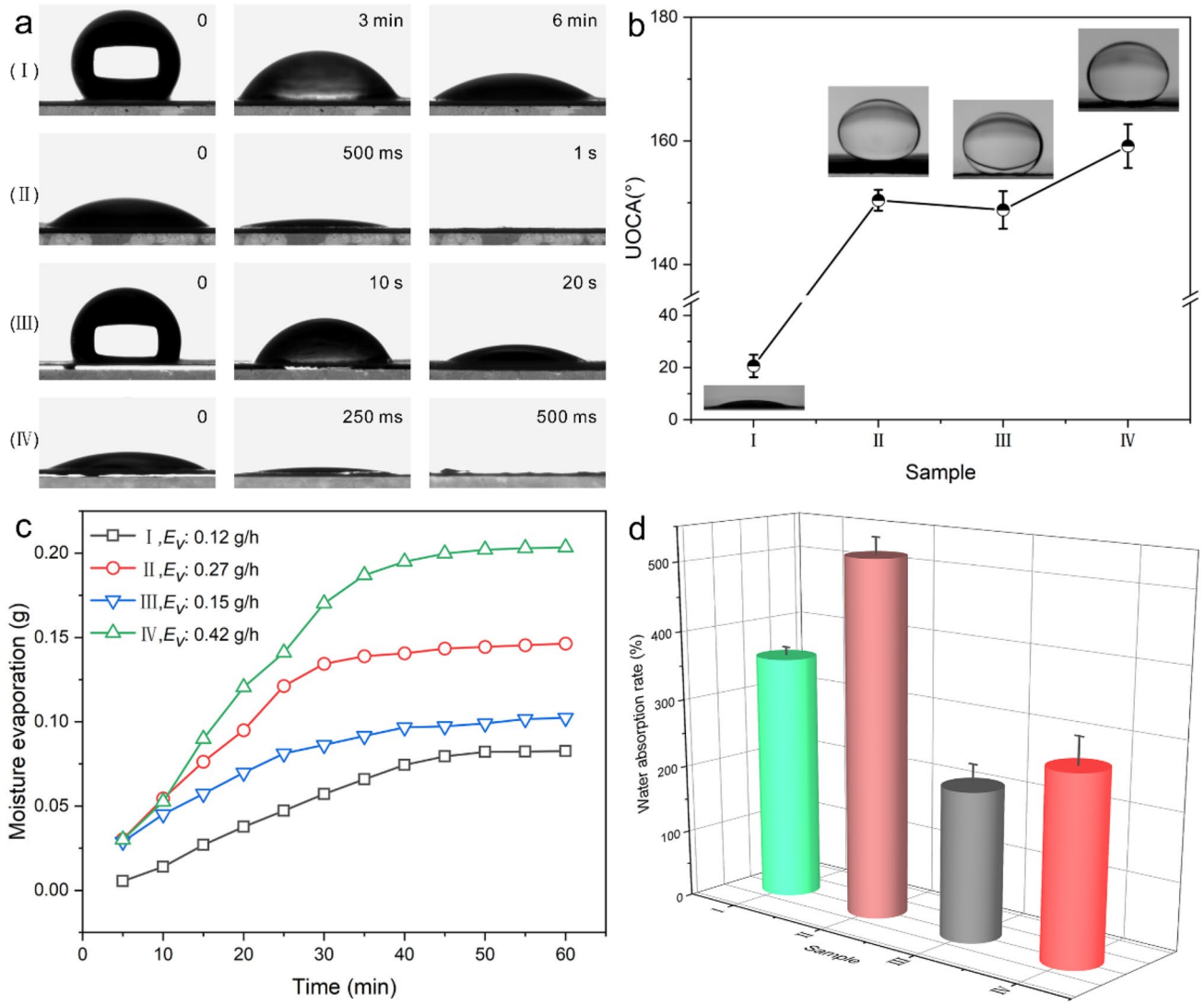

Fig. 2 (**a**) The dynamic process of water droplets (4 μL) in air penetrating the membranes, (**b**) the underwater oil contact angle (UOCA), (**c**) variation in the moisture evaporation as a function of time, and (**d**) the water-absorption rate of the membranes under different treatments: (I) electrospinning, (II) plasma treatment with O_2, (III) wrapped with APTES, and (IV) grafted with SiO_2

slightly from 790 to 828 nm compared to the electrospun PU membrane (Fig. S1). Furthermore, the thickness of the membrane has no further significant improvement, and the thickness of electrospun PU membrane and SiO_2/PU membrane were 85.998 ± 5.876 μm and 91.431 ± 3.250 μm, respectively, based on the cross section in the SEM image (Fig. S2). The hydrophilicity of the membrane was promoted with the decrease of the initial WCA (23.3°, Fig. 2a IV), and the UOCA increased to 159.2° (Fig. 2b IV). Simultaneously, the membrane also exhibited an extremely high moisture-evaporation rate (0.42 g/h, Fig. 2c IV). The water-absorption capacity of the membrane grafted with SiO_2 was much greater than that of the membrane wrapped with APTES, reaching 273%. The corresponding data for water-absorption rate of the membranes under different treatments were shown in Table S1. On the other hand, the water-absorption capacity of the membrane grafted with SiO_2 was drastically lower than that of the untreated membrane, as displayed in Fig. 2d IV.

To further investigate the reason for the change in the wettability of the membrane, the surface chemical composition was surveyed by XPS, FTIR and EDS analysis. Figure 4a depicted the elemental changes of the membrane with different treatments in the XPS. Compared with electrospun PU membrane, the XPS spectra of the plasma treatment membrane revealed characteristic peaks of O1s shifted from 532.24 to 532.74 eV, indicating a conversion from $–CH_2CH_2C(O)O–$ to $–CH_2CHOH–$ (Fig. S3b I–II). After the plasma treatment with O_2, the peak of hydroxyl group (–OH) at 3670/cm was displayed in the FTIR spectra

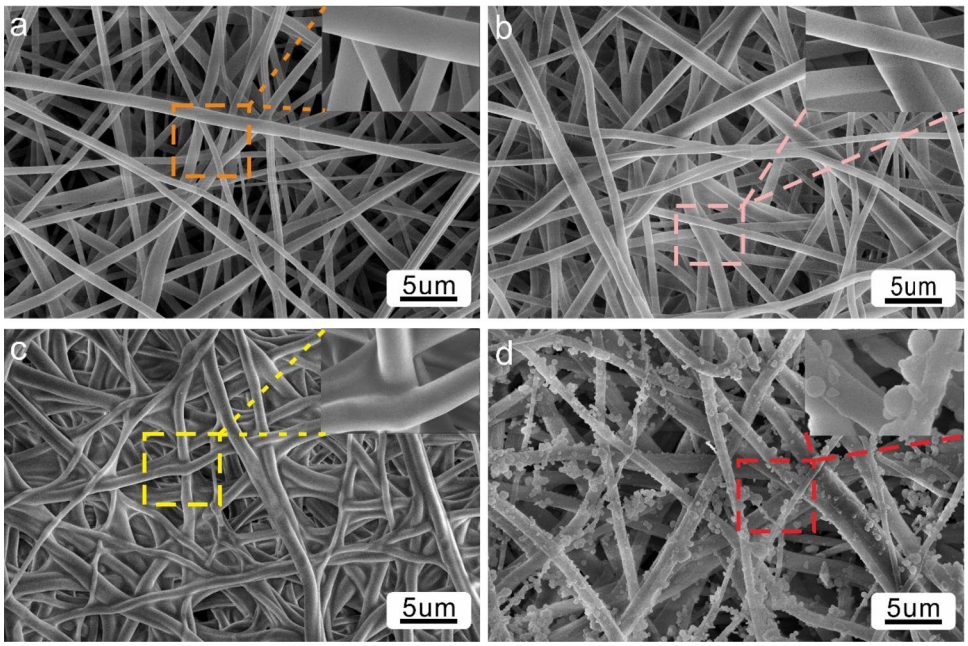

Fig. 3 FE-SEM images of the membranes under different treatments: (**a**) electrospinning, (**b**) plasma treatment with O_2, (**c**) wrapped with APTES, and (**d**) grafted with SiO_2

(Fig. 4b I–II, it indicated that the plasma generated by the O_2 created the hydrophilic active site on the PU molecular chain [42]. With the treatment of APTES, it could be found the characteristic peak at 399.20 eV (N1s) corresponding to $–CH_2CH_2CH_2NH–$ (Fig. S3a III). Furthermore, the intensity of O1s shifted to 532.49 eV with a corresponding molecular formula of $(–Si(CH_3)_2O–)n$ (Fig. S3b III). In addition, the presence of Si2s (153.20 eV) and Si2p (102.40 eV, Fig. 4a III and Fig. S3c III) peaks, which are indicative of $(–Si(CH_3)_2O–)n$ and $(–Si(CH_3)_2O–)n$, were also detected in the XPS spectra. Besides, the EDS analysis of the fibers depicted the occurrence of Si element (Fig. S4a, b and Fig. 4c), and the elemental mapping of the membrane treated by APTES exhibited that the Si element could be found all over the fiber surface (Fig. 4d). This suggested that APTES was successfully coupled to the membrane's fiber surface [43]. Nevertheless, the characteristic peak of –OH group was disappeared in the FTIR spectra, yet the stretching absorption peak of N–H was still present at 3315/cm, moreover, the groups of silane-hydrolysis products (e.g., Si–OH and Si–O–Si) were not observed (Fig. 4b III). It explained the decline in hydrophilicity after the coupling of APTES, due to loss of the hydrophilic groups and the absence of hydrolysis to produce new hydrophilic groups [44]. In addition, when SiO_2 particles gathered on the fiber surface, the N1s XPS spectrum showed overlapping peaks (Fig. S3a IV), which included $–CH_2CH_2CH_2NH–$ (399.40 eV) and (-C(O)NH-)n (401.10 eV) molecular formulas. Meanwhile, the feature of O1s was slightly shifted (532.40 eV, Fig. S3b IV). Combined with the apparent change in the characteristic peak of Si2p (103.00 eV, Fig. 4a IV and Fig. S3c IV), the molecular formula corresponding to the elements of O and Si was converted to SiO_2, which was consistent with the result of FTIR spectrum, and the characteristic peaks of Si–OH group and Si–O-Si group appeared at 956/cm and 790/cm, respectively, as shown in Fig. 4b IV. On the other hand, the Si element of the membrane grafted with SiO_2 was significantly increased from 1.46 to 4.88% (Fig. S4c), moreover, the roughness (R_q) of the fiber surface was significantly increased from 142 to 476 nm due to the presence of SiO_2 particles (Fig. 5e, f). Consequently, the hydrophilic epidermis conferred by Si–OH group and the rough surface agglomerated by the SiO_2 particles endowed the superhydrophilicity to the membrane (SiO_2/PU membrane) [35, 45]. The particle size and content of the SiO_2 grafted onto the membrane were investigated by controlling the amount of NH_4OH during the synthesis of SiO_2 by the hydrolysis and condensation of TEOS. The particle size of SiO_2 was counted from the SEM images (Fig. 6a–c). As depicted in Fig. 6d, e, with the increase of the amount of NH_4OH, the average particle size of SiO_2 increased from 329 to 538 nm, meanwhile, the content of SiO_2 increased from 2.8 to 4.2%. Furthermore, the particle size and content of SiO_2 grafted onto the membrane would not directly affect the hydrophilicity and underwater oleophobicity of the membrane. As shown in Fig. 6a, c, smaller and less SiO_2 grafted on the fiber surface of the membrane, or more and larger SiO_2 filled in the pore channel of the membrane were not conducive to the improvement of the hydrophilicity and underwater oleophilicity of the membrane. Only if the fiber surface of the membrane was grafted more and bigger SiO_2 (Fig. 6b), the WCA of the membrane was lower than 30° (27.3°), and the

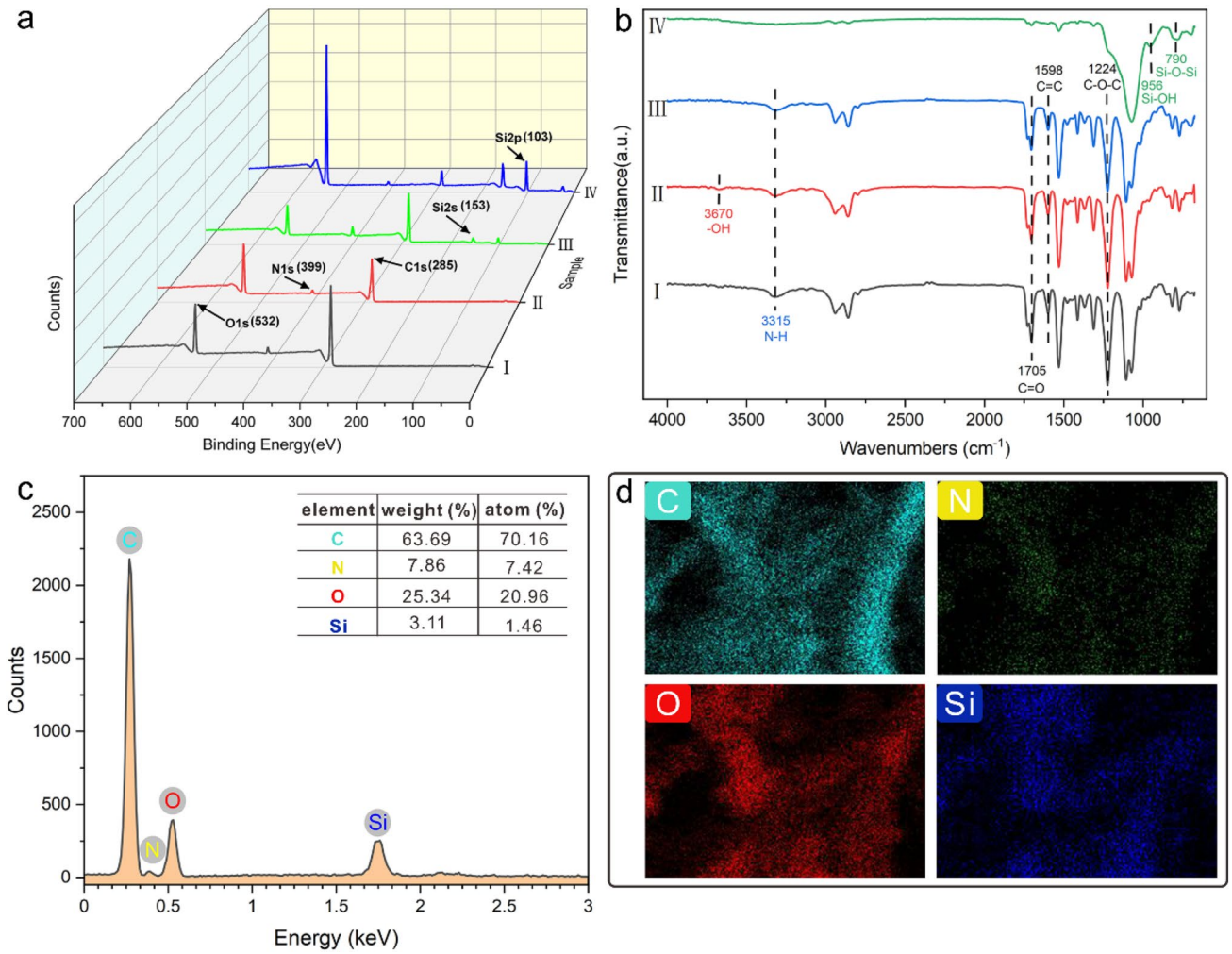

Fig. 4 (**a**) XPS and (**b**) FTIR spectra of the membranes under different treatments: (I) electrospinning, (II) under plasma treatment with O_2, (III) coupled with APTES, and (IV) grafted with SiO_2, (**c**) EDS analysis, and (**d**) the elemental mapping images of the membrane coupled with APTES

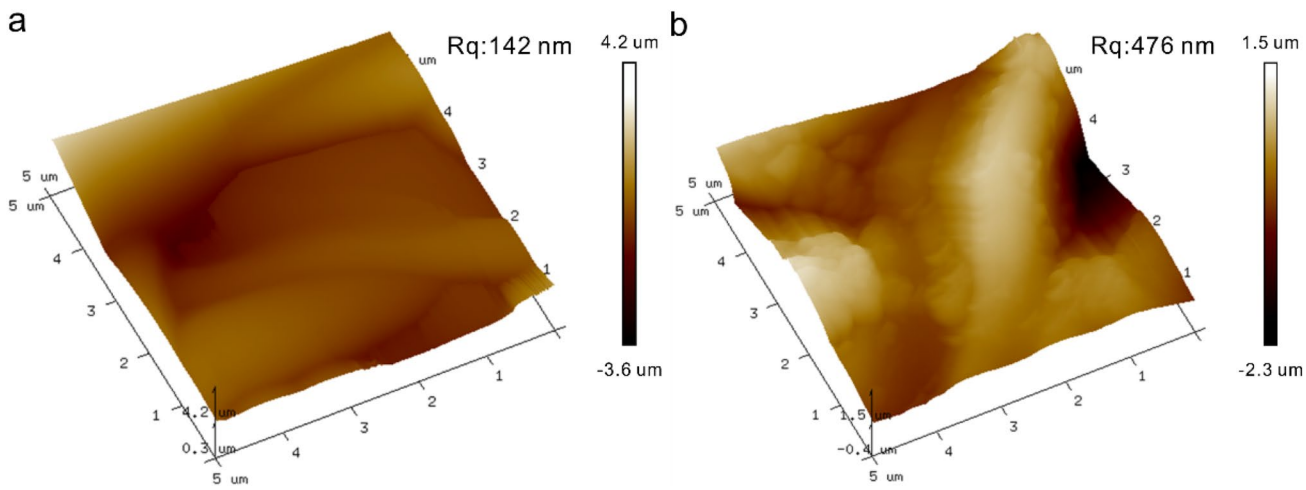

Fig. 5 AFM images of (**a**) electrospun membrane and (**b**) SiO_2/PU membrane

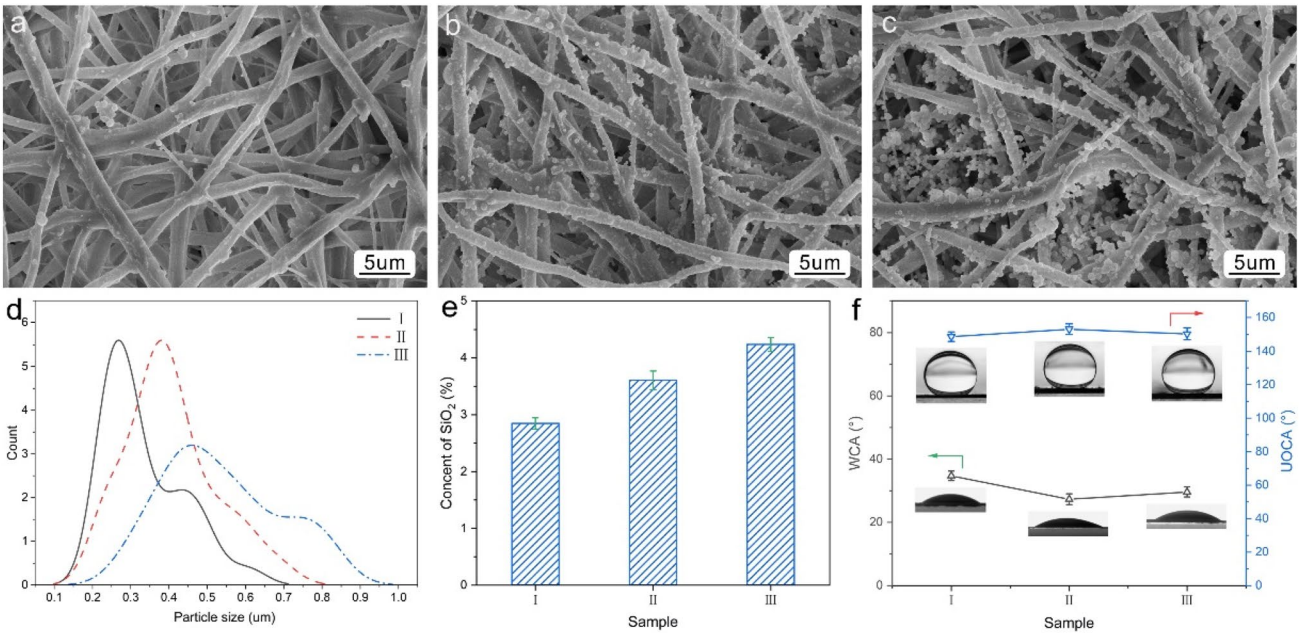

Fig. 6 The FE-SEM images of the membrane grafted with SiO_2 synthesized at different amounts of NH_4OH: (**a**) 0.05 mL, (**b**) 0.1 mL and (**c**) 0.2 mL, (**d**) particle size and (**e**) content of SiO_2 synthesized at different amounts of NH_4OH: (I) 0.05 mL, (II) 0.1 mL, and (III) 0.2 mL, (**f**) WCA and UOCA of the membrane grafted with SiO_2 synthesized at different amounts of NH_4OH: (I) 0.05 mL, (II) 0.1 mL, and (III) 0.2 mL

UOCA was higher than 150° (153.1°), and the membrane became superhydrophilic and underwater superolehydropilic (Fig. 6f).

3.2 The Underwater Olephobicity of SiO_2/PU Membrane

The prepared membrane had exhibited extreme olephobicity to dichloromethane under water with the UOCA of 159.2° in Fig. 2b IV. Simultaneously, as the dichloromethane droplet (8 μL) was squeezed by the needle, the droplet remained subcircular and did not penetrate the membrane, and then when the droplet was lifted, the droplet moved with the needle, indicating that the droplet would not adhere to the membrane in the water (Fig. 7a) [15]. Meanwhile, the dichloromethane (dyed with oil red O) could be rolled over the surface of the membrane immersed in the water, it inferred the low adhesion of the membrane to the oil in the water [5]. Although dichloromethane does not belong to oil, it would obviously contaminate the membrane material if the membrane was not super hydrophilic and underwater super oleophobic. As shown in Fig. S5, dichloromethane would adhere to the water-wetted membrane (Fig. S5a), and it could be found that dichloromethane would contaminate the membrane when the membrane was removed from the water (Fig. S5b). In addition, most oils have a lower density than water, and when these oils contacted with the membrane immersed in water, these oils would float up under the effect of buoyancy, which made it difficult to accurately reflect the underwater oleophobicity of the membrane. Therefore, dichloromethane was utilized to describe the underwater super oleophobicity by the rolling over the surface of the membrane immersed in water, as displayed in Video S1 and Fig. 7b. Moreover, SiO_2/PU membrane possessed underwater superoleophobicity to different kinds of oils, including dichloromethane, carbon tetrachloride, bromobenzene and nitrobenzene, and the UOCA of these oils varied from 155.9 to 159.7° (Fig. 7c). In addition, the underwater oil sliding angle (UOSA) of the membrane to these oils was investigated in the ddddddx. 7d, the UOSA of the oils were below 10° and remained between 4.0 and 4.6°, denominating that the oils with higher density than water could roll on the surface of the membrane [46]. Furthermore, as depicted in Video S2, the prewetted-SiO2/PU membrane immersed in peanut oil showed no absorption of the substance, and the peanut oil dropped from the membrane surface (Fig. 8a). In addition, the membrane surface was not sticky after being washed with water, and the peanut oil was escaped from the membrane surface in the water (Fig. 8b). These suggested that the underwater self-cleaning property of SiO_2/PU membrane [37]. When the prewetted-SiO_2/PU membrane contaminated by motor oil was put into water, the oil spots quickly decreased in size and formed into spherical droplets, and the oil spots floated quickly in the water from the membrane surface (Fig. 8c, d and Video S3), illustrating that the fouling resistance of SiO_2/PU membrane to oil-in-water [47].

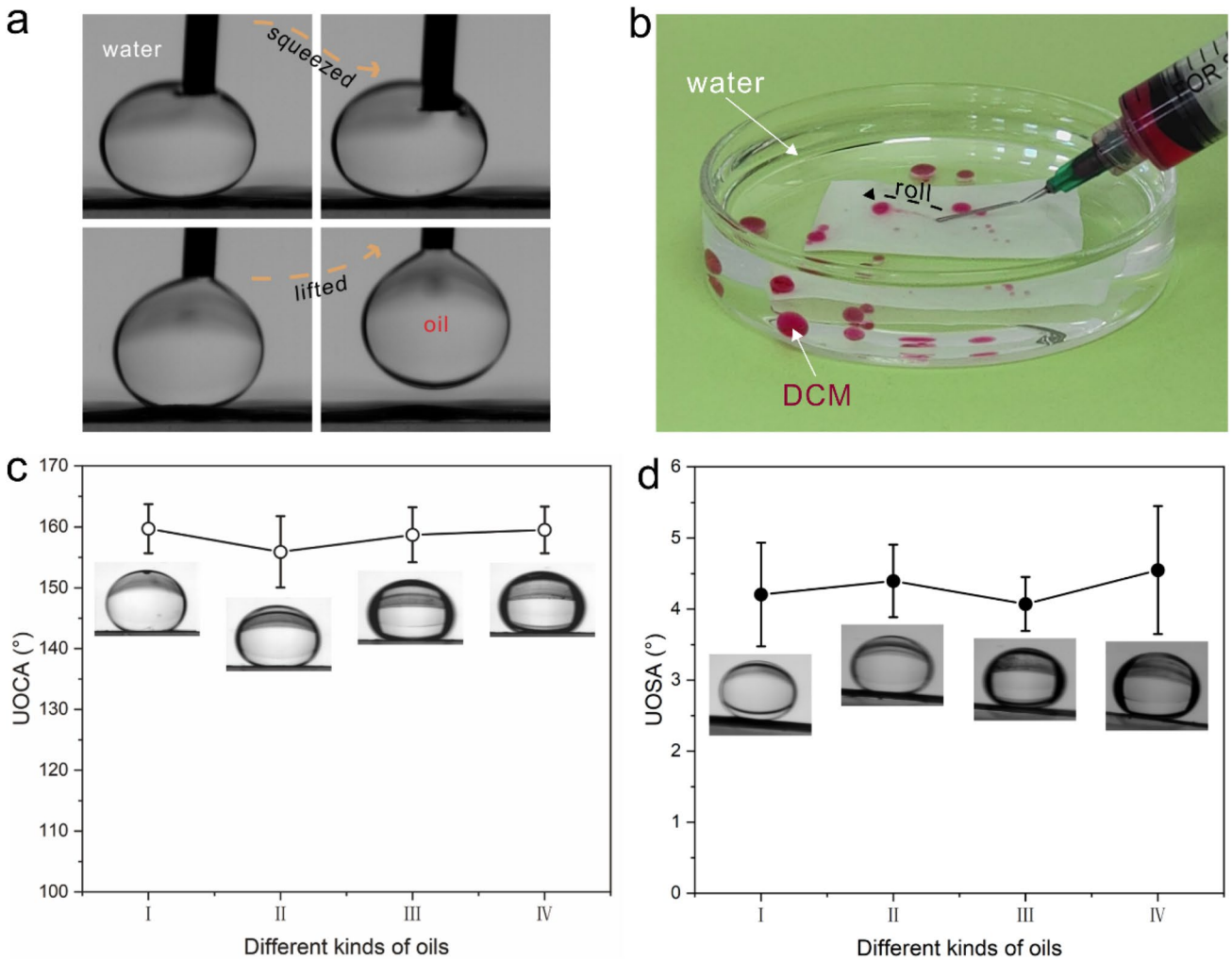

Fig. 7 (**a**) Photograph of dichloromethane being squeezed and lifted on the membrane in water, (**b**) photograph of dichloromethane (dyed with oil red O) rolled over the surface of the membrane immersed in water (**c**) underwater oil contact angle (UWOCA), and (**d**) underwater oil sliding angle (UOSA) of the membrane to the different kinds of oils: (I) dichloromethane, (II) carbon tetrachloride, (III) bromobenzene, and (IV) nitrobenzene

3.3 Oil-In-Water Emulsion Separation of SiO_2/PU Membrane

Due to its special wettability (including superhydrophilicity and underwater superoleophobicity), the SiO_2/PU membrane has excellent resistance to oil contamination and self-cleaning properties in water, making it a potential solution for treating oil wastewater, especially oil-in-water emulsions, which are difficult to separate due to the oil being distributed in the form of small droplets [48]. As seen in Fig. 9a and Video S4, the peanut oil-in-water emulsion (2:100 by volume) prepared with anionic surfactant (SDBS, 1.2 mmol/L) was separated by the SiO_2/PU membrane under the influence of gravity. The emulsion was milky white and turbid and contained numerous oil droplets when observed under an optical microscope (Fig. 9b). The size of the oil droplets ranged from 2.172 to 15.709 μm (Fig. 9c), which was larger than the pore size of the SiO_2/PU membrane (mean of 1.202 μm, Fig. S6b). The sieving effect of the pore channels caused the oil droplets' interfacial membrane to be destabilized by the squeezing or cutting of the fibers in the membrane [9], leading to the aggregation of the droplets into larger ones [49]. The water's repulsion on the surface of the SiO_2/PU membrane to the oil droplets prevented them from penetrating the membrane [17]. However, for electrospun-PU membranes with an average pore size of 3.417 μm, emulsified oils distributed in the aqueous phase with smaller particle sizes will permeate through the membrane with the water (Fig. S6a). When the membrane was grafted with SiO_2, the pore size was significantly reduced and the porosity decreased from 70.55 to 63.14% (Fig. S7),

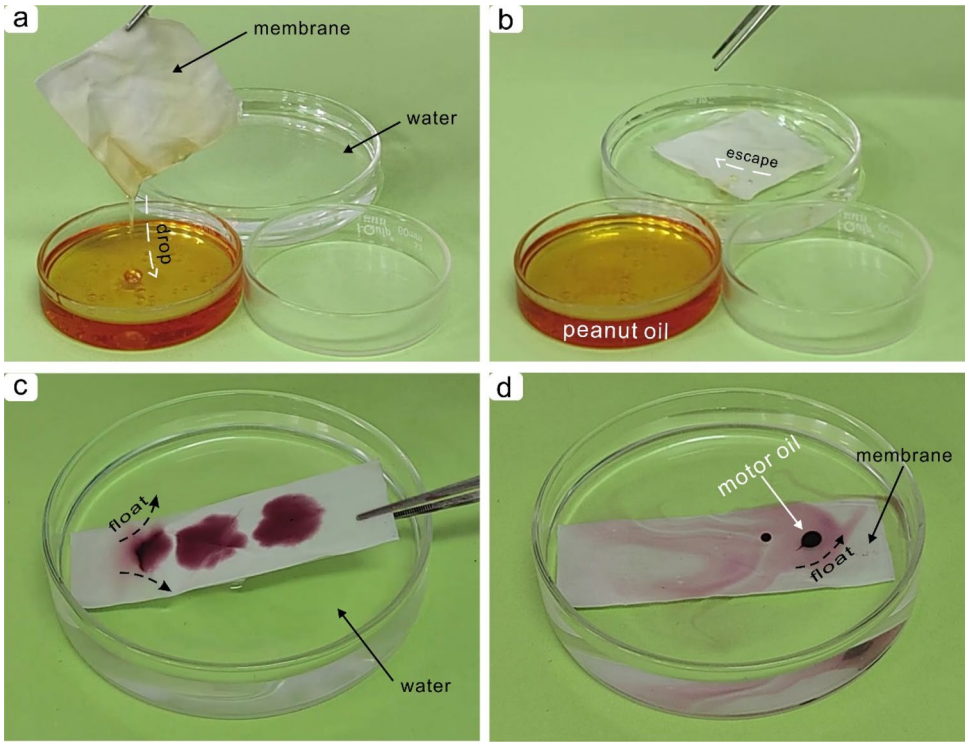

Fig. 8 The fouling resistance of the membrane to peanut oil (**a**, **b**) and motor oil (**c**, **d**) in water

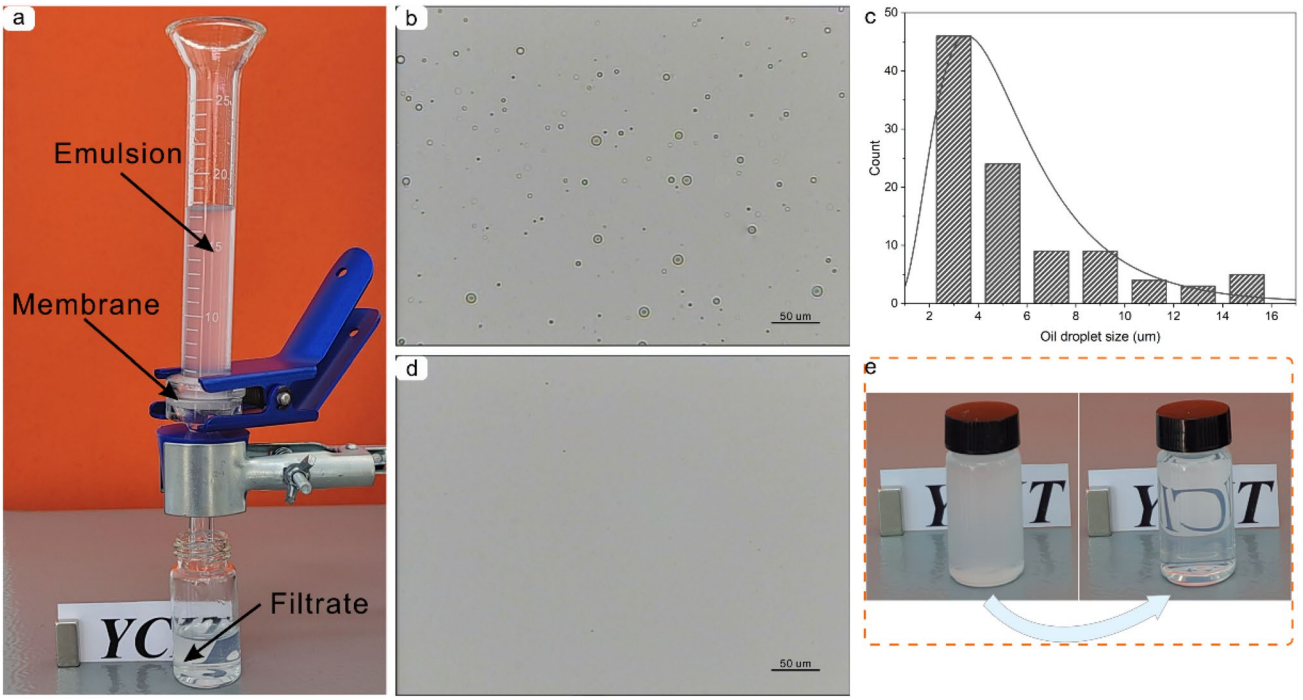

Fig. 9 (**a**) Photo of the oil-in-water emulsion separation with the membrane under gravity, (**b**) photo of the emulsion before the membrane separation, (**c**) photo of the filter after the membrane separation, (**d**) optical-microscope photograph, and (**e**) oil-droplet size of the emulsion before the membrane separation, and (**e**) optical-microscope photograph of the filter after the membrane separation

resulting in a decrease in the water-absorption rate. After membrane separation, the transparent filtrate was obtained and it was difficult to observe the oil droplets in the filtrate (Fig. 9d, e). The variation in separation flux through the membrane to separate oil-in-water emulsion as a function of separation time over a cycle of 30 min was depicted in

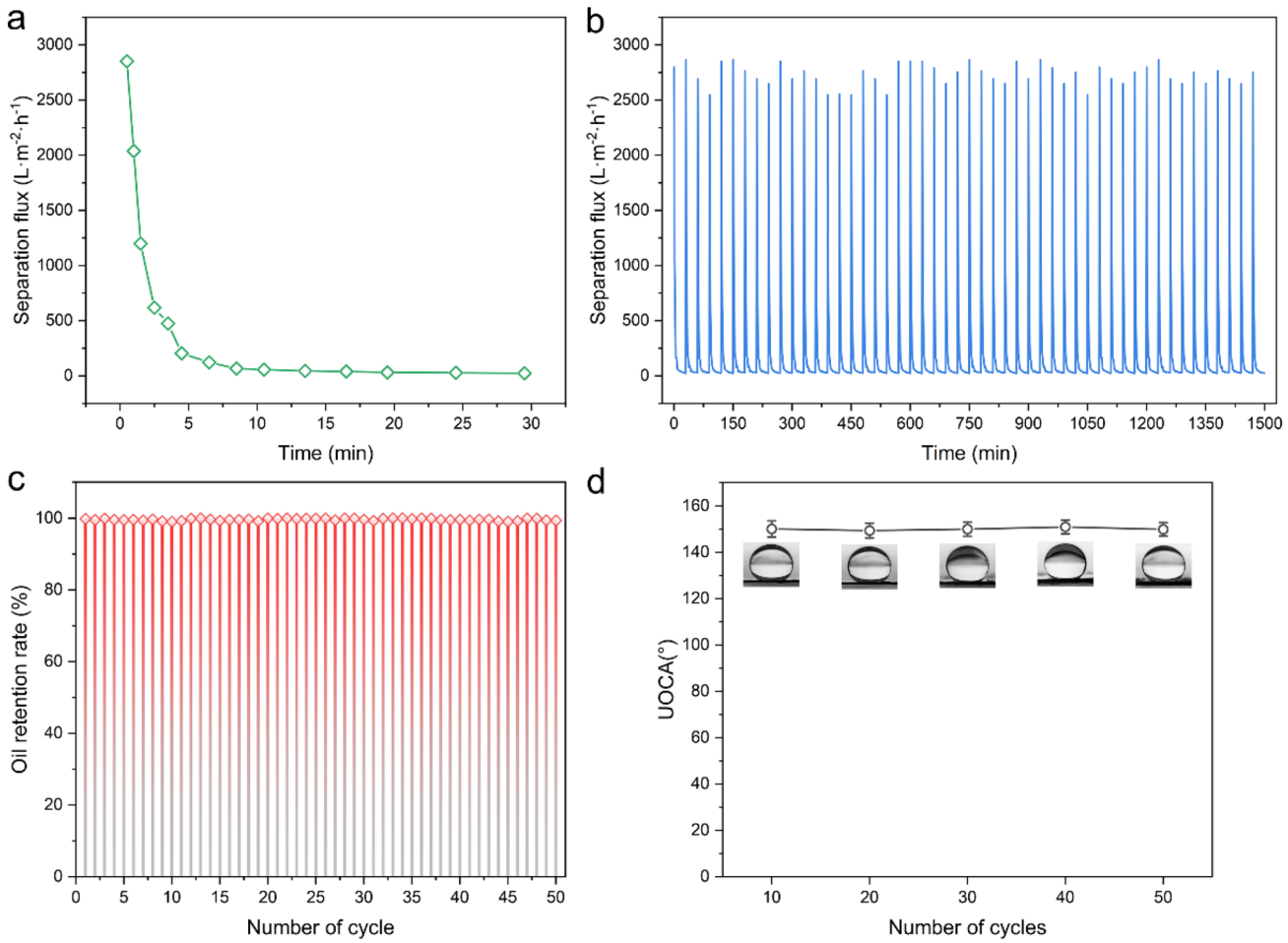

Fig. 10 Separation flux through the membrane to separate oil-in-water emulsion during (**a**) 30 min (1 cycle) and (**b**) 1500 min (50 cycles), (**c**) oil-retention rate of the membrane for the separation of oil-in-water emulsion at different cycles, and (**d**) UOCA of the membrane after the separation of oil-in-water emulsion at different cycles

Fig. 10a. Under the influence of gravity, the separation of oil-in-water emulsion gradually slowed down, indicated by the gradual decrease of the separation flux with time. This was due to the reduced effect of gravity as the emulsion height decreased [50], and the oil droplets adhering to the surface of the membrane made it difficult for the water to penetrate the pore channels of the membrane [51]. And the separation time for the oil-in-water emulsion have been increased to 1500 min (50 cycles, Fig. 10b), the initial separation flux varied from 2546 to 2864 L/m^2/h, and the final separation flux was maintained at 25 L/m^2/h. Furthermore, the stability study of the membrane was investigated by the oil-retention rate and UOCA at different separation cycles. Even after 50 cycles of membrane separation, the oil-retention rate of the membrane for the peanut oil-in-water emulsion remained higher than 99.0% (Fig. 10c). Simultaneously, the membrane still exhibited underwater superoleophobicity with the UOCA fluctuating between 152.5 and 154.7° after the cyclic separation (Fig. 10d).

4 Conclusion

In summary, the electrospun PU membrane was treated with oxygen plasma to introduce active sites (–OH groups), then the fibers were coupled with APTES to make them adhesive. This allowed for the clustering of hydrophilic silica particles on the fiber surface, forming a rough structure and a hydrophilic epidermis to create a superhydrophilic membrane. The initial WCA of the resultant membrane was 23.3°, and the membrane had a moisture-evaporation rate of 0.42 g/h and a water-absorption capacity of 273%. In addition, it showed excellent underwater oleophobicity, with oil droplet not adhering to the membrane in water. Furthermore, the membrane had a UOCA of 155.9 to 159.7° and a UOSA of 4.0 to 4.6° for different oils, meaning that oils with higher density than water could roll on the surface of the membrane in water. The prepared membrane was found to be highly resistant to oil and was able to self-clean when immersed in water. The oil-in-water emulsion with oil-droplet sizes above

2.172 μm, when prepared with anionic surfactant, can be separated from the aqueous phase by the superhydrophilic membrane under gravity. During the cyclic separation of the membbrane for the oil-in-water emulsion (50 cycles), the initial separation flux varied from 2546 to 2864 L/m^2/h, and the final separation flux was maintained at 25 L/m^2/h. Furthermore, the oil-retention rate of the membrane for the peanut oil-in-water emulsion remained higher than 99.0%. Simultaneously, the membrane still exhibited underwater superoleophobicity with the UOCA fluctuating between 152.5 and 154.7° after the cyclic separation.

Supplementary Information The online version contains supplementary material available at https://doi.org/10.1007/s12221-024-00526-3.

Acknowledgements The work was supported by the school level research projects of Yancheng Institute of Technology (xjr2021053) and the Jiangsu Agricultural Science and Technology Innovation Fund (CX(21)3086).

Data Availability All the data that support the findings of this study are available in this manuscript.

Declarations

Conflict of Interest The authors declare that they have no known competing financial interests or personal relationships that could have appeared to influence the work reported in this paper.

References

1. M.N. Islam, B. Yildirim, J. Maryska, F. Yalcinkaya, J. Indus. Text. **52** (2022)
2. W.F. Zhang, R.X. Qu, X.Y. Li, Y.N. Liu, Y. Wei, L. Feng, J. Mater. Chem. A **7**, 27156 (2019)
3. P. Wang, M. Wang, T. Song, J. Chen, X. Liu, X. Liu, Y. You, H. Song, K. Li, Y. Li, W. Feng, X. Yang, J. Water Process Eng. **51**, 103358 (2023)
4. L.Y. Zhang, Y. He, P.Y. Luo, L. Ma, Y. Fan, S.H. Zhang, H. Shi, S.S. Li, Y.L. Nie, J. Mater. Chem. A **8**, 4483 (2020)
5. X.W. Huang, S. Zhang, W. Xiao, J.C. Luo, B. Li, L. Wang, H.G. Xue, J.F. Gao, J. Membr. Sci. **614**, 118500 (2020)
6. D. Wang, S. Mhatre, J. Chen, X. Shi, H. Yang, W. Cheng, Y. Yue, G. Han, O.J. Rojas, Carbohydr. Polym. **299**, 120119 (2023)
7. T.M. Zhang, R.Y. Guo, G.B. Ying, Z.Y. Lu, C. Peng, M.X. Shen, J.F. Zhang, Mater. Horiz. **9**, 1536 (2022)
8. X.F. Feng, Z.X. Yu, R.X. Long, Y.X. Sun, M. Wang, X.H. Li, G.Y. Zeng, Sep. Purif. Technol. **247**, 116945 (2020)
9. B. He, Y.J. Ding, J.Q. Wang, Z.K. Yao, W.H. Qing, Y.J. Zhang, F. Liu, C.Y.Y. Tang, J. Membr. Sci. **581**, 105 (2019)
10. X. Ma, C. Wang, H. Guo, Z. Wang, N. Sun, P. Huo, J. Gu, Y. Liu, J. Mater. Sci. **57**, 6474 (2022)
11. Y. Liao, M. Tian, R. Wang, J. Membr. Sci. **543**, 123 (2017)
12. D.C. Zhong, X.Y. Wang, J.J. Wang, Surf. Coat. Technol. **460**, 129421 (2023)
13. A. Suhaimi, E. Mahmoudi, R. Latif, K.S. Siow, M.H.M. Zaid, A.W. Mohammad, M.F.M.R. Wee, J. Water Process Eng. **44**, 102352 (2021)
14. H.X. Guo, Y.W. Ma, P.Z. Sun, S.P. Cui, Z.P. Qin, Y.C. Liang, RSC Adv. **5**, 63429 (2015)
15. L. Zhang, R.R. Gonzales, T. Istirokhatun, Y.Q. Lin, J. Segawa, H.K. Shon, H. Matsuyama, Sep. Purif. Technol. **272**, 118922 (2021)
16. N. Wang, Y.Y. Zhai, Y.Y. Yang, X. Yang, Z.G. Zhu, Chem. Eng. J. **354**, 463 (2018)
17. X.M. Lu, Y.L. Peng, H.R. Qiu, X.R. Liu, L. Ge, Desalination **413**, 127 (2017)
18. Z.Z. Wei, J.Y. Gu, Y.X. Ye, M.Q. Fang, J.P. Lang, D. Yang, Z.J. Pan, Surf. Coat. Technol. **381**, 125147 (2020)
19. D.M. Correia, C. Ribeiro, V. Sencadas, G. Botelho, S.A.C. Carabineiro, J.L.G. Ribelles, S. Lanceros-Méndez, Prog. Org. Coat. **85**, 151 (2015)
20. V.V.T. Padil, N.H.A. Nguyen, Z. Rozek, A. Sevcu, M. Cernik, Surf. Coat. Technol. **271**, 32 (2015)
21. R. Reis, L.F. Dumee, A. Merenda, J.D. Orbell, J.A. Schutz, M.C. Duke, Desalination **403**, 3 (2017)
22. N. Bhouri, F. Debbabi, A. Merghni, E. Rohleder, B. Mahltig, S. Ben Abdessalem, J. Ind. Text. **51**, 6353S (2022)
23. T.T.A. Owad, E.A.A. Siddig, R.E.M. Salih, Y. Zhang, C.L. Wang, Y. Xu, J. Zhang, Surf. Interfaces **32**, 102081 (2022)
24. F. Ghorbani, A. Zamanian, J. Polym. Eng. **39**, 526 (2019)
25. Z.W. Zeng, Y. Liu, L.L. Long, J.S. He, Y. He, L.L. Wang, G. Yang, X.H. Zhang, F. Shen, Y.Z. Zhang, Surf. Coat. Technol. **434**, 128193 (2022)
26. B.S. Shen, C.X. Du, W. Wang, D. Yu, J. Mater. Sci. **57**, 1474 (2022)
27. Y. Yi, H. Tu, X. Zhou, R. Liu, Y. Wu, D. Li, Q. Wang, X.W. Shi, H.B. Deng, J. Hazard. Mater. **371**, 165 (2019)
28. R.R. Tian, G.R. Hu, X.W. Ou, M.B. Luo, J.Y. Li, J. Chem. Phys. **153**, 124705 (2020)
29. B.S. Shen, C.X. Du, W. Wang, D. Yu, Fibers Polym. **23**, 3386 (2022)
30. C. Li, H. Lai, Z.J. Cheng, J.J. Yan, L.H. Xiao, L. Jiang, M.Z. An, Chem. Eng. J. **385**, 123924 (2020)
31. R. Ding, T.J. Chen, Q.Z. Xu, R. Wei, B. Feng, J. Weng, K. Duan, J.X. Wang, K. Zhang, X.D. Zhang, ACS Biomater. Sci. Eng. **6**, 842 (2020)
32. H.H. Gu, G.Q. Li, P.P. Li, H.L. Liu, T.T. Chadyagondo, N. Li, J. Xiong, Appl. Surf. Sci. **512**, 144 (2020)
33. X.Y. Gu, N. Li, H.H. Gu, X. Xia, J. Xiong, J. Appl. Polym. Sci. **135**, 46360 (2018)
34. Y. Cai, D.Y. Chen, N.J. Li, Q.F. Xu, H. Li, J.H. He, J.M. Lu, J. Mater. Chem. A **7**, 1629 (2019)
35. Kimdaseul, K. Jeongmin, J. Jaeyoung, H. Minsik, S.S. Min, J.-H. Kim, Fibers Polym. **23**, 2365 (2022)
36. H. Gu, L. Gao, G. Li, N. Li, J. Xiong, J. Ind. Text. **51**, 7860S (2021)
37. Q. Wang, Y.J. Fu, X.X. Yan, Y.J. Chang, L.L. Ren, J. Zhou, Appl. Surf. Sci. **412**, 10 (2017)
38. L. Xia, L. Li, Y. Xiao, F. Xiao, W. Ji, S. Jiang, H. Wang, Carbohydr. Polym. **300**, 120269 (2023)
39. S.Z. Liu, Q. Zhang, L.Y. Fan, R. Wang, M.J. Yang, Y. Zhou, Ind. Eng. Chem. Res. **59**, 11713 (2020)
40. S. Xiao, H.L. Wang, F.C. Hu, H.J. Sue, Polymer **137**, 209 (2018)
41. E. Brunengo, L. Conzatti, R. Utzeri, S. Vicini, M. Scatto, E.V. Falzacappa, M. Castellano, P. Stagnaro, J. Mater. Sci. **54**, 14367 (2019)
42. F. Bohlooli, A. Anagri, S. Mori, Carbon **196**, 327 (2022)
43. M.I.H. Mondal, M.K. Islam, F. Ahmed, J. Nat. Fibers **19**, 5451 (2022)
44. Y.L. Nie, S.H. Zhang, Y. He, L.Y. Zhang, Y.Q. Wang, S.S. Li, N. Wang, New J. Chem. **46**, 4734 (2022)
45. B.Z. Lin, S.X. Zhou, Prog. Org. Coat. **106**, 145 (2017)
46. S.S. Li, Y. He, L.Y. Zhang, J.B. Li, Y.L. Nie, H.J. Li, X.Y. Yin, Y. Bai, J. Hazard. Mater. **414** (2021)

47. K. He, H.R. Duan, G.Y. Chen, X.K. Liu, W.S. Yang, D.Y. Wang, ACS Nano **9**, 9188 (2015)
48. W.M. Liu, M.K. Cui, Y.Q. Shen, G.R. Zhu, L. Luo, M.J. Li, J. Li, J. Colloid Interface Sci. **549**, 114 (2019)
49. C.C. Li, X.Y. Chen, J. Luo, F. Wang, G.J. Liu, H.L. Zhu, Y.H. Guo, Separ. Purif. Technol. **259** (2021)
50. Y.I. Guo, M. Li, X. Wen, X.H. Guo, T.T. Zhang, Fibers Polym. **23**, 1906 (2022)
51. I.S. Al-Husaini, A.R.M. Yusoff, W.J. Lau, A.F. Ismail, M.Z. Al-Abri, M.D.H. Wirzal, Chem. Eng. Res. Des. **148**, 142 (2019)